

ARTICLE OPEN



Pacific oceanic front amplifies the impact of Atlantic oceanic front on North Atlantic blocking

Ho-Nam Cheung^{1,2,3}, Nour-Eddine Omrani^{3,4}, Fumiaki Ogawa⁵, Noel Keenlyside^{3,4,6,7}, Hisashi Nakamura⁸ and Wen Zhou⁹

Atmospheric blocking is a crucial driver of extreme weather events, but its climatological frequency is largely underestimated in state-of-the-art climate models, especially around the North Atlantic. While air-sea interaction along the North Atlantic oceanic frontal region is known to influence Atlantic blocking activity, remote effects from the Pacific have been less studied. Here we use semi-idealised experiments with an atmospheric general circulation model to demonstrate that the mid-latitude Pacific oceanic front is crucial for climatological Atlantic blocking activity. The front intensifies the Pacific eddy-driven jet that extends eastward towards the North Atlantic. The eastward-extended Pacific jet reinforces the North Atlantic circulation response to the Atlantic oceanic front, including the storm track activity and the eddy-driven jet. The strengthening of the eddy-driven jet reduces the Greenland blocking frequency. Moreover, the Pacific oceanic front greatly strengthens the stationary planetary-scale ridge in Europe. Together with a stronger northeastward extension of the Atlantic storm track, enhanced interaction between extratropical cyclones and the European ridge favours the occurrence of Euro-Atlantic blocking. Therefore, the North Atlantic circulation response amplified remotely by the Pacific oceanic front substantially increases Euro-Atlantic blocking frequency while decreasing Greenland blocking frequency.

npj Climate and Atmospheric Science (2023)6:61; <https://doi.org/10.1038/s41612-023-00370-x>

INTRODUCTION

Blocking refers to a warm-core anticyclone remaining quasi-stationary throughout the extratropical troposphere for at least 4–5 days^{1–3}. Blocking persistently deflects the large-scale westerlies and embedded weather systems, and hence a blocking anticyclone often triggers extreme weather events, such as long-lasting cold spells, heat waves, droughts and floods^{4–8}. Accurate prediction of blocking is useful in preparing for extreme weather events. However, general circulation models (GCMs) are deficient in simulating the climatology of large-scale atmospheric circulation and blocking activity, especially over the North Atlantic^{9–11}. The multi-model ensemble mean of the winter Euro-Atlantic blocking frequency in CMIP5 and CMIP6 models is only around one-third to half of the observed climatology^{12–14}. Improved physical understanding of North Atlantic blocking is thus needed¹⁴.

North Atlantic blocking occurs most frequently downstream of the mid-latitude storm track¹⁵ (see also shading in Fig. 1a), where the poleward transport of heat and vorticity by transient eddies is strongest. Transient eddies, including developing extratropical cyclones, are crucial for the formation of blocking^{16,17}. The development of extratropical cyclones is closely related to lower-tropospheric baroclinicity associated mainly with changes in the meridional sea surface temperature (SST) gradient and the land-sea thermal contrast¹⁸. Climatologically, the SST gradient is sharpest along the western boundary currents in the North Atlantic and Pacific Oceans; the associated sharp SST gradients are called mid-latitude oceanic fronts, referring to the Gulf Stream front in the North Atlantic and the Kuroshio Extension front in the

North Pacific. The bias in the winter Euro-Atlantic blocking frequency is partly related to substantial SST bias along the Gulf Stream^{19,20}.

Large-scale SST anomalies are associated mainly with changes in surface heat fluxes involving two-way air-sea interaction^{21–23}. On one hand, atmospheric temperature and humidity can directly influence SST by influencing turbulent heat fluxes according to bulk aerodynamic formulae²⁴. Because the ocean has a larger thermal inertia than the atmosphere, atmospheric forcing could have a cumulative effect on the ocean²⁵, such as the time-lagged impact of the North Atlantic Oscillation on the North Atlantic oceanic circulation^{26–30}. On the other hand, recent studies have revealed the potential impacts of mid-latitude oceanic fronts and their associated air-sea interaction on the large-scale tropospheric circulation via their influence on turbulent heat fluxes and extratropical cyclones^{31–34}. O'Reilly et al.³⁵ further demonstrated that a weaker SST gradient in the North Atlantic oceanic front could weaken poleward eddy heat transport by extratropical cyclones. This implies weaker synoptic forcing on the eddy-driven jet over the North Atlantic, and this affects the variability of the jet, leading to lower blocking frequency over the Euro-Atlantic sector. The correction of the bias along the Gulf Stream could greatly reduce the bias of Euro-Atlantic blocking^{19,20}. In addition to the Euro-Atlantic sector, blocking frequency has a secondary peak over the Greenland sector^{15,36} (see also shading in Fig. 1a). Whereas Euro-Atlantic blocking occurs downstream of the climatological Atlantic storm track, Greenland blocking occurs at its poleward flank³⁶. The meridional shift of the

¹School of Atmospheric Sciences & Southern Marine Science and Engineering Guangdong Laboratory (Zhuhai), Zhuhai, China, Sun Yat-sen University, Zhuhai, China. ²Guangdong Province Key Laboratory for Climate Change and Natural Disaster Studies, Guangzhou, China. ³Bjerknes Centre for Climate Research, University of Bergen, Bergen, Norway. ⁴Geophysical Institute, University of Bergen, Bergen, Norway. ⁵Graduate School of Science, Hokkaido University, Sapporo, Japan. ⁶Nansen Environmental and Remote Sensing Center, Bergen, Norway. ⁷A.M. Obukhov Institute of Atmospheric Physics, RAS, Moscow, Russia. ⁸Research Center for Advanced Science and Technology, The University of Tokyo, Tokyo, Japan. ⁹Department of Atmospheric and Oceanic Sciences & Institute of Atmospheric Sciences, Fudan University, Shanghai, China.

[✉]email: hoffmancheung@gmail.com; Nouredine.Omrani@uib.no

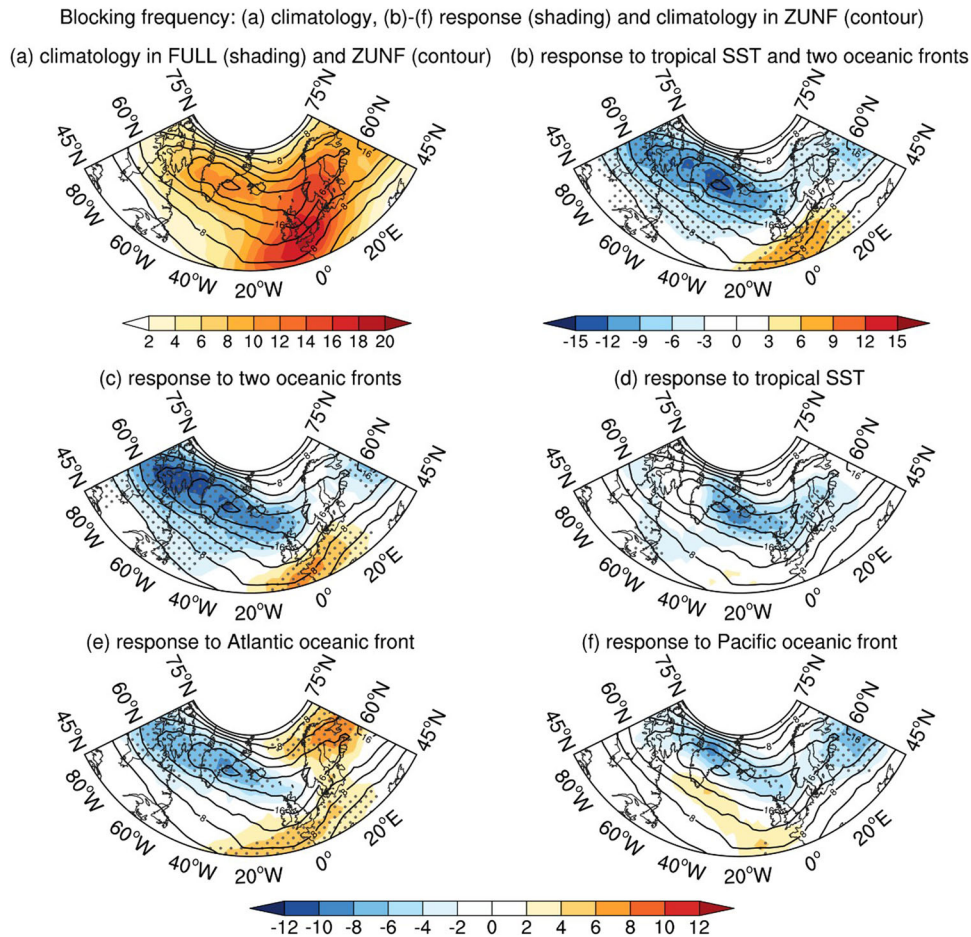


Fig. 1 Impacts of the oceanic fronts and the tropical SST on the winter (DJF) climatological blocking frequency across the Euro-Atlantic region. Spatial distribution of the blocking frequency in (a) the FULL run (with realistic SST in the Northern Hemisphere and tropics; shading) and the ZUNF run (with zonally uniform tropical SST and without oceanic fronts; contour interval: 4%), **b–f** response in semi-idealised experiments (i.e. difference between the experiments and the ZUNF run; shading) and the climatology in the ZUNF run (contours: **b** tropical SST and two oceanic fronts (FULL run), **c** two oceanic fronts (EXT_ALL run), **d** tropical SST (TROP_ALL run), **e** Atlantic oceanic front (EXT_ATL run), and **f** Pacific oceanic front (EXT_PAC run). Stippling in (b)–(f) indicates differences exceeding the 95% confidence interval based on the two-tailed Student's *t*-test.

Atlantic oceanic front is coupled with the meridional displacement of the Atlantic storm track³⁷ and the change in Greenland blocking activity³⁸.

The large-scale atmospheric circulation over the North Atlantic is also influenced by remote forcing from the Pacific^{39–44}. For example, El Niño events enhance the positive phase of the Pacific–North America teleconnection pattern and shift Pacific blocking eastward⁴⁵. Wintertime El Niño and La Niña tend to be followed by the negative and positive phase, respectively, of the North Atlantic Oscillation in late winter⁴⁶. Backward-trajectory analysis has also revealed that moisture from the Pacific contributes to the formation of Atlantic blocking⁴⁷. Therefore, a comprehensive understanding of North Atlantic blocking should include the less studied cross-basin teleconnection between the Pacific and Atlantic, where the underlying physical mechanism remains unclear.

Here we use semi-idealised atmospheric-only experiments of MAECHAM5 (the Middle Atmosphere configuration of the fifth generation of the Hamburg version of the ECMWF model) in ref. ⁴⁴, to examine the individual and joint impacts of the tropical SST and the mid-latitude oceanic fronts over the North Atlantic and North Pacific on winter Atlantic blocking activity under realistic orography: (1) the zonally uniform tropical SST/no front

(ZUNF) run prescribes zonally uniform SST at each latitude; (2) the semi-idealised experiments prescribe realistic SST in specific ocean basins, such that the difference between (2) and (1) gives an atmospheric response to a specific SST pattern (see methods).

Large-scale atmospheric circulation characteristics can be simulated well in atmospheric models by prescribing the climatological SST. Indeed, the climatological SST is associated with ocean circulation characteristics. For example, strong SST gradients in the northwestern Atlantic and northwestern Pacific reflect heat convergence along the boundary between the subpolar and subtropical gyres. The aim of our experiments is to understand how the ocean circulation characteristics associated with the climatological SST over the mid-latitudes and tropics can maintain the climatological atmospheric circulation. These characteristics are reflected in: (1) the mid-latitude oceanic front associated with the ocean western boundary currents, which affects the lower-level baroclinicity and synoptic-scale eddies; (2) the zonally asymmetric SST associated with Bjerknes feedback in the tropics, which affects the Walker circulation, the Hadley circulation, the subtropical jet, and even the extratropical atmospheric circulation. These SSTs are associated with atmosphere-ocean coupling.

RESULTS AND DISCUSSION

Oceanic impacts on Atlantic blocking frequency

The run with realistic SST forcing in the Northern Hemisphere and tropics (FULL; Fig. 1a) basically captures the observed blocking frequency distribution, although the simulated blocking frequency is generally higher and the maximum centre in the mid-latitudes is shifted southward to $\sim 50^\circ\text{N}$ compared to the NCEP/NCAR reanalysis⁴⁸ climatology (Supplementary Fig. 1). The temporal evolution of Euro-Atlantic and Greenland blocking events in the FULL run is found comparable to that of blocking events in the reanalysis (Supplementary Figs. 2–3). The above results demonstrate the ability of MAECHAM5 to simulate Atlantic blocking.

The semi-idealised experiments provide insights into the impact of different SST forcing on the climatological Atlantic blocking frequency. When zonally uniform SST is prescribed in the tropics and the mid-latitude oceanic fronts are greatly weakened (the ZUNF run), the blocking frequency distribution is markedly different from that in the FULL run (Fig. 1a). The ZUNF run simulates much lower blocking frequency over the mid-latitude Euro-Atlantic (10.5% in ZUNF vs. 18.6% in FULL at 50°N , 0.5°W , which is the peak in the FULL run) and much higher blocking frequency around Greenland (24.9% in ZUNF vs. 11.3% in FULL at 65°N , 37.5°W , which is the secondary peak in the FULL run); the primary blocking centre is shifted to Greenland. In other words, the tropical SST and mid-latitude oceanic fronts jointly increase the mid-latitude Euro-Atlantic blocking frequency by 77.1% and reduce the Greenland blocking frequency by 54.4% (Fig. 1a). Without the tropical SST and oceanic fronts, North Atlantic blocking tends to recur near Greenland rather than in the mid-latitude Euro-Atlantic domain as observed.

The impact of SST on the spatial distribution of the North Atlantic blocking frequency is primarily through the contribution from the mid-latitude oceanic fronts. The blocking frequency response to the joint influence of the Atlantic and Pacific oceanic fronts (Fig. 1c) largely resembles the response in the FULL run (Fig. 1b). In contrast, the blocking frequency response to the tropical SST is characterized by a reduction in Greenland and Euro-Atlantic blocking (Fig. 1d), where this response is mainly by the tropical Indo-Pacific SST (figure not shown). We further decompose the influence of the mid-latitude oceanic fronts on blocking into the contributions from the Atlantic and the Pacific. On one hand, the Atlantic oceanic front acts to increase the blocking frequency over Eurasia and reduce it over Greenland (Fig. 1e). On the other hand, the Pacific oceanic front acts to reduce the blocking frequency over western Russia and Greenland and slightly increase it over the mid-latitude Euro-Atlantic (shading in Fig. 1f). It appears that the Atlantic and Pacific oceanic fronts coherently influence Atlantic blocking.

The two mid-latitude oceanic fronts jointly increase the peak of Euro-Atlantic blocking frequency in the FULL run by 70.7% (the maximum response is 7.42%), which accounts for 91.7% of the response in the FULL run (70.7 out of 77.1%). The remaining 8.3% of the response in the FULL run is attributed to the influence of tropical SST in the presence of mid-latitude oceanic fronts. For the impact of the oceanic fronts on Euro-Atlantic blocking frequency, 58.8% is due to the sole impact of the Atlantic oceanic front, and the remaining 41.2% is related to the Pacific oceanic front. Meanwhile, the oceanic fronts and the tropical SST reduce the peak of Greenland blocking frequency by 42.1% and 26.4%, respectively, which accounts for 77.4% and 48.5%, respectively, of the response in the FULL run. For the Greenland blocking frequency response to the two oceanic fronts, 75.9% can be explained by the sole impact of the Atlantic oceanic front, and the remaining 24.1% is related to the Pacific oceanic front. Overall, in terms of the SST forcing considered in this study, the oceanic fronts primarily affect the Atlantic blocking frequency, while the tropical SST further enhances the response of blocking frequency

to the oceanic fronts. In the following we will explain how the oceanic fronts jointly enhance the occurrence of Euro-Atlantic blocking and reduce the occurrence of Greenland blocking.

Oceanic impacts on dynamic processes of blocking events

To understand how the Atlantic and Pacific oceanic fronts jointly affect North Atlantic blocking, we first investigate the role of the oceanic fronts in setting up the dynamic processes of the observed blocking events. Here, the blocking events are diagnosed by the geopotential height tendency equation at 500-hPa due to vorticity flux convergence^{17,49,50} (see “diagnostic equations” in Methods). The vorticity flux convergence is decomposed into its high-frequency (representing synoptic-scale activities), low-frequency, and cross-frequency components to assess their contribution to the development of Atlantic blocking events (Eq. 2 in Methods).

The composited development of Euro-Atlantic blocking events (centred at $45^\circ\text{--}55^\circ\text{N}$ and $10^\circ\text{W--}10^\circ\text{E}$) in the FULL run (with realistic tropical SST and oceanic fronts in the Northern Hemisphere) is characterized by an eastward-propagating wave train-like signal across the North Atlantic (contours in Fig. 2). This wave train-like signal consists of an incipient positive height tendency over eastern Canada, a negative tendency peaking on day–2 over the central Atlantic, and another positive tendency peaking on day–1 over the eastern Atlantic and Europe (contours in Fig. 2). This time evolution indicates successive intensification of a trough over the central Atlantic and a ridge over Europe during the development of Euro-Atlantic blocking. This trough-ridge couplet slowly moves eastward during the development of blocking. The successive intensification of this trough-ridge couplet in the FULL run is attributed partly to the high-frequency forcing associated with a synoptic-scale wave train across the North Atlantic (shading in Fig. 2a–e).

Moreover, low-frequency forcing is crucial for the enhancement of the European ridge (shading in Fig. 2f–j), which agrees with previous studies that the formation of blocking downstream of a storm track is partly due to the low-frequency eddies^{51–53}. Indeed, the European ridge intensifies before the synoptic-scale wave train approaches it. This indicates the role of a pre-existing ridge in the development of Euro-Atlantic blocking. The dynamic evolution of a Euro-Atlantic blocking event in the FULL run is similar to that in the reanalysis (contours in Fig. 2 vs. contours in Supplementary Fig. 4), except that in the reanalysis the high-frequency forcing makes a larger contribution to the development of blocking (Supplementary Fig. 4a–e). Overall, the development of an Euro-Atlantic blocking event involves interaction between a synoptic-scale wave train propagating across the North Atlantic and a pre-existing European ridge, which is consistent with previous studies^{50,53–55}.

The synoptic-scale wave train across the North Atlantic in the FULL run is most pronounced from day–3 to day–2. The wave train is similar in the run with the two realistic mid-latitude oceanic fronts and the run with realistic Atlantic mid-latitude oceanic front, where the wave train signal is slightly stronger in the former run (Supplementary Fig. 5b–c). The wave train is, however, not apparent in either the run with only realistic tropical SST or the run without tropical SST and SST-fronts (Supplementary Fig. 5d–e), suggesting the crucial role of the mid-latitude oceanic fronts in the precursory North Atlantic signal of Euro-Atlantic blocking.

To further depict the impact of oceanic fronts on the development of Euro-Atlantic blocking, the budget of the geopotential height tendency is evaluated at $10^\circ \times 10^\circ$ across the blocking high centre (green box in Fig. 2), as shown in Fig. 3. In the FULL run, the maximum high-frequency and low-frequency forcing at the blocking high centre is $+35 \text{ m day}^{-1}$ on day–1 and between day–2 and day–1, respectively (red and blue lines in Fig. 3a). The cross-scale term makes a much smaller contribution

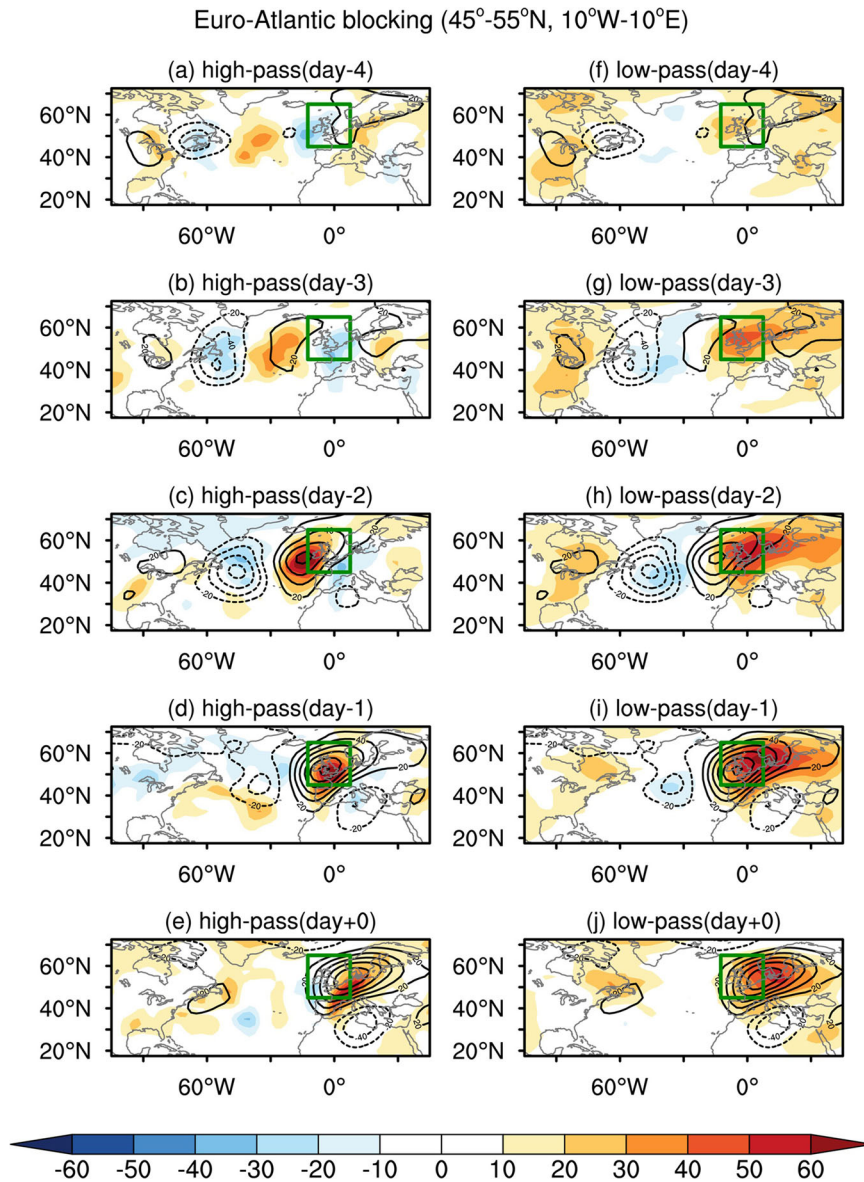


Fig. 2 Development of Euro-Atlantic blocking in the FULL run. Contribution of high-frequency and low-frequency components of vorticity flux convergence (shading) to the daily geopotential height tendency at 500 hPa (contours) from day–4 to day+0 of composited Euro-Atlantic blocking events in the FULL run: **a–e** high-frequency component and **f–j** low-frequency component. Unit: $m \text{ day}^{-1}$.

(green line in Fig. 3a). When both the mid-latitude oceanic fronts and tropical SST asymmetry are removed (the ZUNF run), the peak values of the high-frequency and low-frequency forcing are greatly reduced by 49% and 29%, to $+18 \text{ m day}^{-1}$ and $+25 \text{ m day}^{-1}$, respectively (red and blue lines in Fig. 3b). The peak of high-frequency forcing in the run with two realistic oceanic fronts and the run with a realistic Atlantic oceanic front ($+30 \text{ m day}^{-1}$) is close to that in the FULL run (red line in Fig. 3c–d), while the corresponding peak value is slightly weaker in the run with a realistic Pacific oceanic front ($+25 \text{ m day}^{-1}$; red line in Fig. 3e) and even weaker in the run with realistic tropical SST ($+20 \text{ m day}^{-1}$; red line in Fig. 3f). The two oceanic fronts are thus found to greatly enhance the high-frequency forcing responsible for the formation of Euro-Atlantic blocking, where the major contribution is from the Atlantic oceanic front.

The peak values of the low-frequency forcing in the run with the two realistic oceanic fronts and in the run with realistic tropical SST ($+35 \text{ m day}^{-1}$; blue line in Fig. 3c, f) are comparable to that of the FULL run (blue line in Fig. 3a). However, this forcing is

somewhat weaker in the run with a realistic Atlantic oceanic front and the run with a realistic Pacific oceanic front ($+25 \text{ m day}^{-1}$; blue line in Fig. 3d, e). Moreover, the development of Euro-Atlantic blocking in the run with realistic tropical SST is associated with an intensification of a low-frequency wave-like signal from North America to Europe (Supplementary Fig. 5i). Such a wave-like signal over the North Atlantic is different from the FULL run (Fig. 2h) and the run with the two realistic oceanic fronts (Supplementary Fig. 5g). Hence, we deduce that the low-frequency forcing in the FULL run is mainly due to the joint effect of the Atlantic and Pacific oceanic fronts.

The composite development of Greenland blocking events in the FULL run is characterized by a wave train-like signal extending northeastward over the mid-latitude North Atlantic (contours in Fig. 4), which originates from the southwestward flank of the developing Greenland blocking high. This wave train-like signal consists of a positive height tendency over the east coast of North America, a negative height tendency around Newfoundland and another positive height tendency south of Greenland most

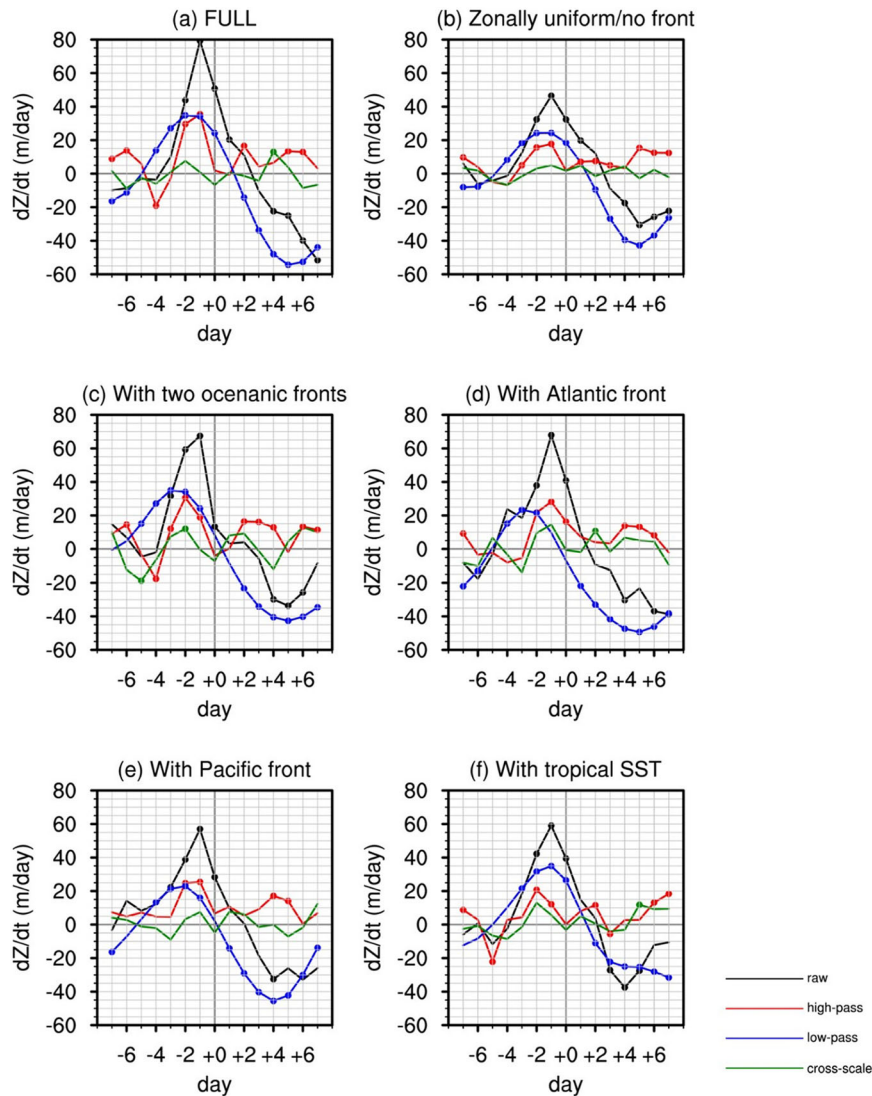


Fig. 3 Impacts of the oceanic fronts and the tropical SST on dynamic processes associated with the evolution of Euro-Atlantic blocking centre. Daily geopotential height tendency at 500 hPa and the contribution from different dynamic processes averaged over $10^\circ \times 10^\circ$ across the blocking high centre from day -7 to day $+7$ of the composited Euro-Atlantic blocking events in the **a** FULL run, **b** ZUNF run, **c** EXT_ALL run, **d** EXT_ATL run, **e** EXT_PAC run and **f** run with realistic SST over the entire tropics (TROP_ALL run), where the black line indicates the raw geopotential height tendency, and the red, blue and green lines indicate the contributions from the high-frequency, low-frequency and cross-scale component of the vorticity flux divergence, respectively. Unit: $m \text{ day}^{-1}$. Dots indicate that the term on a specific date is significantly different from zero, according to the 95% confidence interval of a one-tailed t -test.

apparent on day -1 (Fig. 4d). This wave train-like signal is primarily due to high-frequency dynamics (shading in Fig. 4a–e), suggesting that the wave train-like signal is attributable to the synoptic-scale wave train propagating from North America to the southern portion of the developing blocking high (shading in Fig. 4a–e). Meanwhile, the intensification of the northern portion of the Greenland blocking high is due to low-frequency forcing (shading in Fig. 4f–j). The dynamics of the Greenland blocking event in the FULL run is similar to that in the reanalysis, where the synoptic forcing is stronger (Supplementary Figs. 6 and 7a).

The synoptic-scale wave train involved in the development of Greenland blocking is reproduced only in the run with the realistic oceanic fronts and the run with a realistic Atlantic oceanic front (Supplementary Fig. 7b–c). Compared to the runs with the oceanic fronts, the extratropical cyclone over the east coast of North America is much weaker in the runs without the realistic oceanic fronts (Supplementary Fig. 7d–e). Meanwhile, the northern portion of the developing Greenland blocking high is associated with

somewhat weaker low-frequency forcing in the run without the realistic oceanic fronts (Supplementary Fig. 7g–j). It appears that the oceanic fronts are crucial for both the high-frequency and low-frequency dynamics of realistic Greenland blocking events.

The development of a Greenland blocking high in the FULL run is initiated by low-frequency forcing, with its maximum on day -3 ($+42 m \text{ day}^{-1}$; blue line in Fig. 5a). The contribution from high-frequency forcing peaks on day -2 ($+35 m \text{ day}^{-1}$; red line in Fig. 5a), associated with the northeastward migration of the synoptic-scale wave train from North America to Greenland (shading in Fig. 4a–e). The cross-scale term plays only a minor role in the evolution of the Greenland blocking high (green line in Fig. 5a). In the ZUNF run, the contributions from high-frequency forcing ($+25 m \text{ day}^{-1}$) and the low-frequency forcing ($+20 m \text{ day}^{-1}$) are reduced by 30% and more than 50%, respectively (red and blue lines in Fig. 5b). Comparatively, the high-frequency forcing in the run with the two oceanic fronts ($+30 m \text{ day}^{-1}$; red line in Fig. 5c) is slightly weaker than that in the

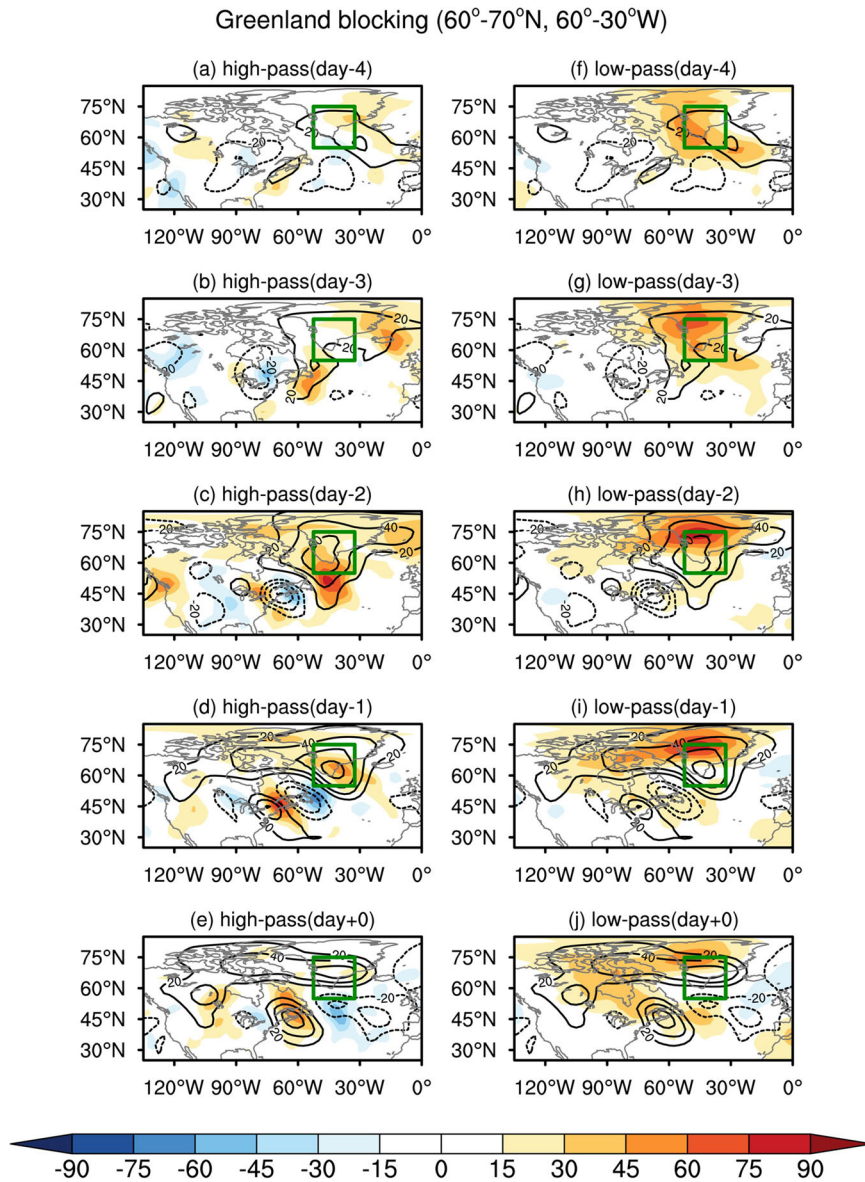


Fig. 4 Development of Greenland blocking in the FULL run. Contribution of high-frequency and low-frequency components of vorticity flux convergence (shading) to the daily geopotential height tendency at 500 hPa (contours) from day–4 to day+0 of composited Greenland blocking events in the FULL run: **a–e** high-frequency component and **f–j** low-frequency component. Unit: $m \text{ day}^{-1}$.

FULL run (red line in Fig. 5a). The high-frequency forcing in the run with a realistic Atlantic oceanic front ($+40 \text{ m day}^{-1}$; red line in Fig. 5d) is stronger than that in the FULL run, whereas the high-frequency forcing in the run with a realistic Pacific oceanic front and the run with the realistic tropical SST ($+20 \text{ m day}^{-1}$; red line in Fig. 5d, e) is even smaller than that in the ZUNF run (red line in Fig. 5b). The above results suggest that the Atlantic oceanic front is crucial for enhancing the synoptic-scale wave train over the North Atlantic involved in the development of Greenland blocking.

The low-frequency forcing in the run with two realistic oceanic fronts ($+48 \text{ m day}^{-1}$; blue line in Fig. 5c) is comparable to that in the FULL run during the development of Greenland blocking (blue line in Fig. 5a). The low-frequency forcing in the runs with a realistic Atlantic oceanic front ($+30 \text{ m day}^{-1}$) and the Pacific oceanic front ($+25 \text{ m day}^{-1}$) is smaller than that in the FULL run (blue line in Fig. 5d, e). The low-frequency forcing in the run with the realistic tropical SST ($+20 \text{ m day}^{-1}$; Fig. 5f) is comparable to that in the ZUNF run (Fig. 5b). It appears that the low-frequency

forcing on the development of Greenland blocking is enhanced by the joint effect of the two oceanic fronts.

In short, the two oceanic fronts are crucial for the observed dynamic processes of Euro-Atlantic and Greenland blocking events. First, the Atlantic mid-latitude oceanic front contributes to stronger high-frequency forcing from North America to the North Atlantic prior to the development of Euro-Atlantic and Greenland blocking events. Second, the two oceanic fronts jointly enhance the low-frequency forcing contributing to the development of Euro-Atlantic and Greenland blocking events. We will show that the Pacific oceanic front amplifies the response of Atlantic blocking frequency to the Atlantic oceanic front by influencing the Atlantic storm track and the stationary planetary-scale circulation across the North Atlantic.

Oceanic impacts via the storm track activity

On seasonal timescales, oceanic fronts enhance the meridional contrasts in the release of turbulent heat flux from the ocean to

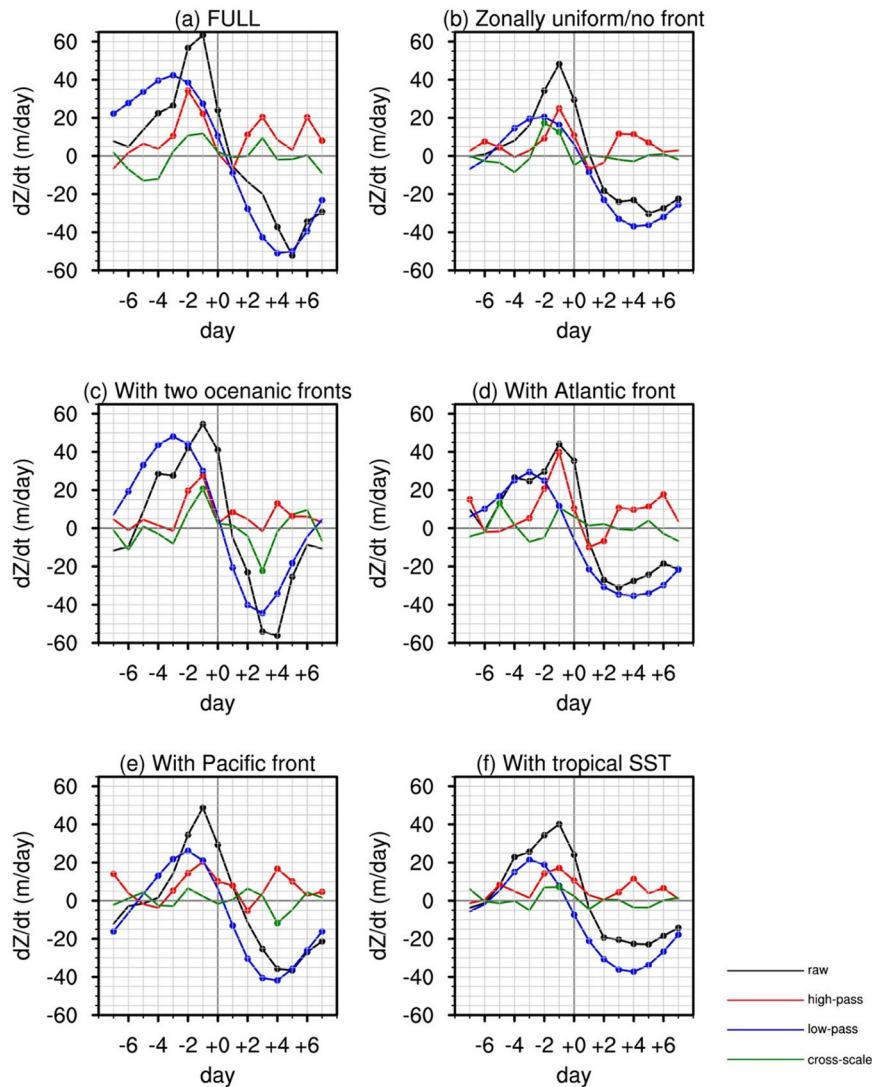


Fig. 5 Impacts of the oceanic fronts and the tropical SST on dynamic processes associated with the evolution of Greenland blocking centre. Daily geopotential height tendency at 500 hPa and its contribution from different dynamic processes averaged over $10^\circ \times 10^\circ$ across the blocking high centre from day -7 to day +7 of the Greenland blocking events: **a** FULL run, **b** ZUNF run, **c** EXT_ALL run, **d** EXT_ATL run, **e** EXT_PAC run and **f** TROP_ALL run, where the black line indicates the raw geopotential height tendency, and the red, blue, and green lines indicate the contribution from the high-frequency, low-frequency and cross-scale component of the vorticity flux divergence. Unit: $m \text{ day}^{-1}$. Dots indicate that the term on a specific date is significantly different from zero, according to the 95% confidence interval of a one-tailed *t*-test.

the atmosphere. The enhanced contrast in sensible heat release maintains a stronger meridional temperature gradient in the lower troposphere^{44,56}, which is necessary for the recurrent development of migratory cyclones and anticyclones to anchor a storm track^{18,57,58}. In addition to the lower-tropospheric baroclinicity, latent heat release from a warm ocean current, such as the Gulf Stream or the Kuroshio Extension, favours the development of extratropical cyclones via increasing diabatic heating^{31,44}. Intensification of extratropical cyclones or storm-track activity is crucial for the development of blocking^{49,50,53}, thus influencing the blocking frequency over the Euro-Atlantic sector⁵⁵.

Extratropical cyclone activity can be measured as storm-track activity^{18,44,59,60}, here defined locally as a root mean square value of the 2.5–8-day band-pass filtered geopotential height at 250 hPa. Climatologically, in the ZUNF run, the North Atlantic storm track extends eastward from the northwestern Atlantic around the oceanic front to Eurasia (contours in Fig. 6). In response solely to the Atlantic oceanic front, the storm-track activity becomes ~35% stronger in the northwestern Atlantic, and this response extends

northeastward towards Europe (Fig. 6a). An enhanced eastward extension of the Atlantic storm track represents more passage of synoptic-scale wave trains towards Eurasia. As will be shown later, the Atlantic oceanic front also slightly enhances the stationary planetary-scale ridge over Europe. Because the occurrence of Euro-Atlantic blocking involves interaction between an extratropical cyclone and a pre-existing European ridge (Fig. 2), the enhanced interaction between extratropical cyclones migrating towards Europe and the European ridge favours more frequent occurrence of Euro-Atlantic blocking (Fig. 1c).

As a downstream response solely to the Pacific oceanic front, Atlantic storm-track activity is enhanced only in the northwestern Atlantic (Fig. 6b), and this response extends slightly farther northeastward but exerts no strong influence on the occurrence of Euro-Atlantic blocking. The two oceanic fronts thus jointly enhance the northeastward extension of Atlantic storm-track activity by ~60% (Fig. 6c), which is almost double the response to the Atlantic oceanic front alone. In contrast, tropical SST plays only a minor role in the storm-track response. Tropical SST enhances

Storm-track activity: response (shading) and climatology in ZUNF (contour)

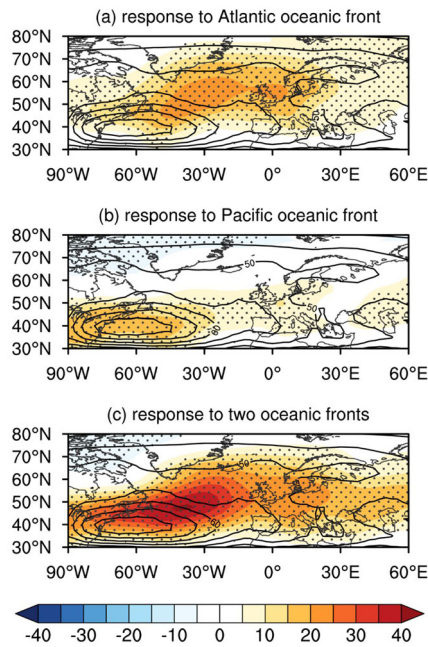


Fig. 6 Impacts of the oceanic fronts on the climatological storm-track activity. Response of the DJF 250-hPa storm-track activity in the sensitivity experiments (shading: m) and the climatology in the ZUNF run (contour interval: 5 m): **a** Atlantic oceanic front (EXT_ATL run), **b** Pacific oceanic front (EXT_PAC run), and **c** those two oceanic fronts (EXT_ALL run).

Atlantic storm-track activity by only $\sim 5\%$, and the storm-track response to the joint influence of the tropical SST and the oceanic fronts is comparable to the response to the two oceanic fronts (figures not shown). Therefore, the Atlantic storm-track response is enhanced by the Atlantic oceanic front, and this response is further amplified by the Pacific oceanic front. Note that the northeastward extension of the Atlantic storm track is also determined by the orographic forcing of the Rockies⁶¹. Though beyond the scope of this study, the possible role of the Rockies in the downstream impact of the Pacific oceanic front on the Atlantic circulation will be discussed later.

Oceanic impacts via mean states

The mid-latitude oceanic fronts enhance transient eddy activity and thereby act to strengthen the eddy-driven jet^{44,58}. The effect of transient eddies on background westerlies can be depicted by the E-vector⁶², where the divergence and convergence of E-vectors represents an acceleration and deceleration, respectively, of the westerlies as the feedback forcing of transient eddies. Specifically, E-vectors based on the 8-day high-pass-filtered wind fields and their divergence are used for assessing the feedback forcing of synoptic-scale cyclonic and anticyclonic eddies on the westerlies as the influence of the oceanic fronts.

The two oceanic fronts enhance the synoptic-wave forcing that strengthens the eddy-driven westerly jets locally, as evidenced by the divergence of the E-vectors (Fig. 7a, b). As the sole response to the Pacific oceanic front, the enhanced E-vectors extend eastward across North America into the North Atlantic (Fig. 7b). The eastward-extending E-vectors indicate the downstream impact of the Pacific eddy-driven jet on the slight enhancement of the Atlantic eddy-driven jet. Specifically, the eastward extension of a stronger Pacific eddy-driven jet corresponds to the stronger westerlies over North America. The intensified lower-tropospheric westerlies impinge on the Rockies, acting to strengthen the mid-

latitude baroclinic eddies and the eddy-driven jet downstream^{63,64}. The above result implies a remote impact of the Pacific oceanic front on the Atlantic eddy-driven jet via enhancing synoptic-wave activity from the North Pacific into the North Atlantic. The enhancements of synoptic-wave activity over the North Atlantic locally by the Atlantic oceanic front and remotely by the Pacific oceanic front are thus coherent. Under the joint influence of the two oceanic fronts, the synoptic-wave activity over the North Atlantic becomes much stronger than it does under the sole influence of either of the two oceanic fronts. The corresponding synoptic forcing leads to a much stronger Atlantic eddy-driven jet (Fig. 7c vs. Fig. 7a, b). Therefore, the climatological North Atlantic circulation is strongly modulated as the joint influence of the Atlantic and Pacific oceanic fronts.

The intensification of the Atlantic eddy-driven jet corresponds to anticyclonic and cyclonic response to the south and north, respectively, of the northeastward-extending jet (Supplementary Fig. 8). This dipolar response resembles the positive phase of the North Atlantic Oscillation⁶⁵. These geopotential height responses also correspond to the enhancement of a stationary planetary-scale trough over the east coast of Canada and a stationary planetary-scale ridge over the eastern Atlantic and Europe, as indicated by the upper-tropospheric eddy geopotential height (as the zonally asymmetric component; Fig. 8). Specifically, the Atlantic geopotential height responses to the Atlantic oceanic front represent a stronger meridional geopotential gradient south of Greenland (Fig. 8a), which corresponds to a stronger westerly jet (Fig. 7a), leading to less reversal of the geopotential gradient and thus lower blocking frequency near Greenland (Fig. 1c). In jointly enhancing the westerly jet south of Greenland by $\sim 60\%$, the Atlantic and Pacific oceanic fronts individually strengthen the westerlies by $\sim 30\%$ and $\sim 15\%$, respectively (Fig. 7a, b). Thus, the Atlantic oceanic front reduces the Greenland blocking frequency by enhancing the Atlantic eddy-driven jet, and the jet response is doubled by the Pacific oceanic front.

The stronger planetary-scale ridge over the eastern Atlantic is favourable for higher blocking frequency over the Euro-Atlantic region. The Atlantic and Pacific oceanic fronts act to strengthen the ridge by $\sim 5\%$ and $\sim 60\%$, respectively (Fig. 8a, b), and they jointly enhance the ridge by $\sim 60\%$ (Fig. 8c). The stronger planetary-scale ridge could be caused partly by more frequent occurrence of Euro-Atlantic blocking. Hence, we also compare the eddy geopotential height response to the oceanic fronts during all DJF days, blocking days, and non-blocking days (Supplementary Fig. 9). As can be seen in Supplementary Figure 9c, such a stronger planetary-scale ridge response is still apparent, when day -7 to day $+7$ of Euro-Atlantic blocking events (45° – 65° N and 30° W– 30° E) are excluded. The eastern Atlantic ridge is not further enhanced by the joint impact of tropical SST and the two oceanic fronts (figure not shown). Therefore, the Pacific oceanic front is crucial for enhancing the eastern Atlantic ridge. Recall that the formation of Euro-Atlantic blocking involves interaction between extratropical cyclones and anticyclones under intensification and a pre-existing ridge near Europe. The Atlantic and Pacific oceanic fronts act to strengthen the Atlantic storm-track activity and the eastern Atlantic planetary ridge, respectively, and it is their joint influence that shapes the Euro-Atlantic blocking activity centre climatologically.

In addition to the oceanic fronts, orographic forcing by the Rockies is also important for the northeastward extension of the Atlantic storm-track and the stationary planetary-wave pattern over the Atlantic^{61,66}. Indeed, the orographic effect of the Rockies on the stationary planetary-wave circulation was found to be sensitive to the orographic forcing of the Tibetan Plateau^{67,68}. Assessing the role of orographic forcing and the two oceanic fronts in climatological blocking activity will require a separate study. Specifically, this future study will investigate the impact of the Rockies and the Tibetan Plateau on the North Atlantic

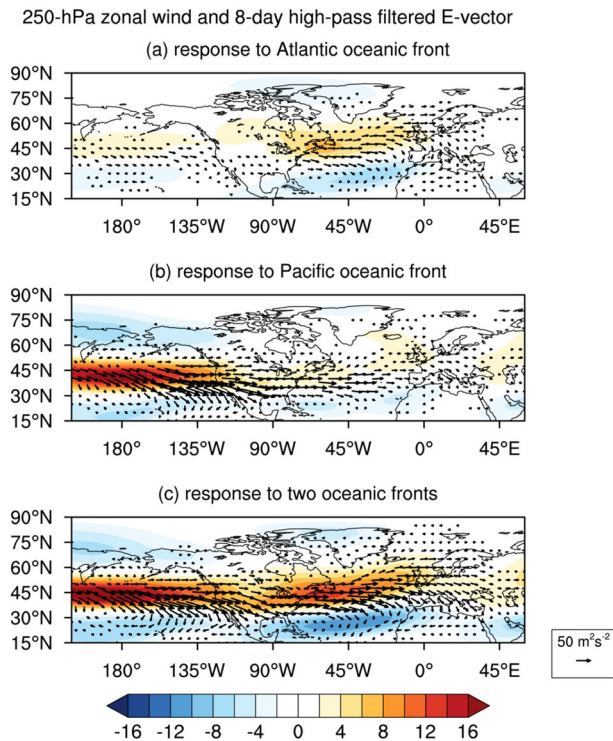


Fig. 7 Impacts of the oceanic fronts on synoptic wave activity. Response of the DJF 250-hPa zonal wind (shading; ms^{-1}) and E-vector (vectors; m^2s^{-2}) in the sensitivity experiments: **a** Atlantic oceanic front (EXT_ATL run), **b** Pacific oceanic front (EXT_PAC run), and **c** two oceanic fronts (EXT_ALL run).

atmospheric response to the Pacific oceanic front, which will provide deeper physical understanding of the remote influence of the Pacific oceanic front on Atlantic blocking.

DISCUSSION

The occurrence of North Atlantic (Euro-Atlantic and Greenland) blocking events involves interaction between the intensification of extratropical cyclones and the planetary-scale ridge near the developing blocking high, where the former factor is due to the high-frequency and low-frequency forcings and the latter factor is related mainly to low-frequency forcing. In this study we have analysed the individual and joint effects of the Atlantic and Pacific oceanic fronts on North Atlantic blocking using semi-idealised atmospheric-only experiments. These experiments isolate the response of the atmosphere to the ocean but not vice versa, where the mid-latitude oceanic fronts are self-sustained by two-way air-sea interaction^{18,21,22,32}.

Without the oceanic fronts (the ZUNF run), blocking tends to occur at the high latitudes with a peak frequency near Greenland. The high-frequency and low-frequency forcings involved in the evolution of North Atlantic blocking events are substantially weaker than in the experiment with realistic SST. In the presence of the Atlantic oceanic front, the upper-tropospheric planetary trough over eastern Canada deepens, the Atlantic eddy-driven jet strengthens, and the Atlantic storm-track activity intensifies and extends northeastward. The storm-track response corresponds to more frequent passage of extratropical cyclones and anticyclones across the North Atlantic. This response leads to stronger synoptic-scale wave trains across the North Atlantic and thereby favours the occurrence of blocking. More frequent interaction between the synoptic wave-train and the stationary planetary-scale ridge over Europe results in more frequent occurrence of Euro-Atlantic blocking. Conversely, because of quasi-geostrophic balance, the

250-hPa eddy geopotential height and Plumb flux

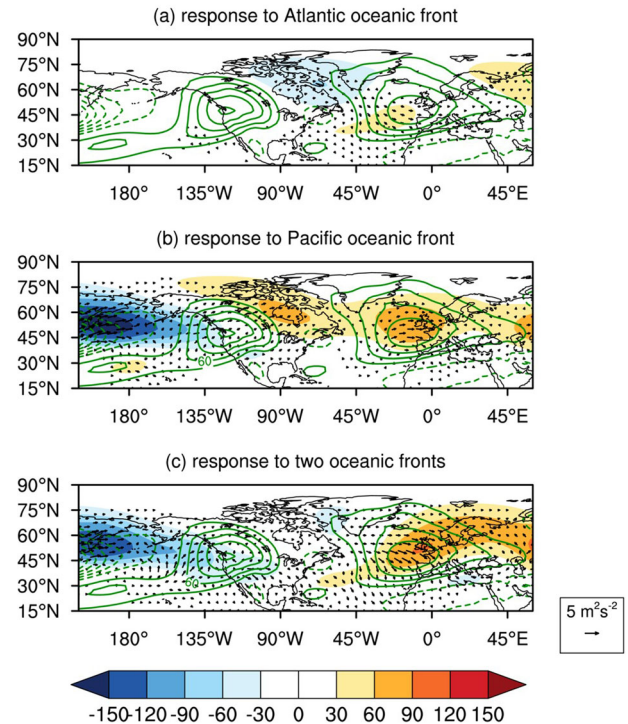


Fig. 8 Impacts of the oceanic fronts on the stationary planetary-scale ridge. Response of the DJF 250-hPa eddy geopotential height (shading; m) and the Plumb flux (vectors; m^2s^{-2}) in the sensitivity experiments: **a** Atlantic oceanic front (EXT_ATL run), **b** Pacific oceanic front (EXT_PAC run), and **c** two oceanic fronts (EXT_ALL run). Green contours indicate the climatology of the eddy geopotential height in the ZUNF run (interval: 30 m).

jet response corresponds to less frequent reversal of the geopotential height gradient, resulting in less frequent occurrence of Greenland blocking. Therefore, the Atlantic oceanic front affects North Atlantic blocking frequency by modulating the storm-track and the eddy-driven jet over the North Atlantic. The impact of the Atlantic oceanic front on North Atlantic blocking is consistent with that found in previous work^{19,20,35,38}.

In addition, we have uncovered the crucial role of the Pacific mid-latitude oceanic front in modulating blocking activity over the North Atlantic. The stationary planetary-scale ridge over the eastern Atlantic becomes stronger in the presence of the Pacific oceanic front, which favours the occurrence of Euro-Atlantic blocking. Under the coexistence of the two oceanic fronts, the responses of the Atlantic storm track and eddy-driven jet are stronger than their responses solely to the Atlantic oceanic front. The stationary planetary-scale ridge response over the eastern Atlantic is comparable to the response solely to the Pacific oceanic front. These responses lead to more substantial increase and decrease in blocking frequency over the mid-latitude Euro-Atlantic and Greenland, respectively, compared to the blocking frequency response solely to the Atlantic oceanic front. Hence, the climatological-mean Atlantic blocking frequency is strongly affected by the joint impacts of the Atlantic and Pacific mid-latitude oceanic fronts, where the Pacific oceanic front acts to amplify the atmospheric response to the Atlantic oceanic front. Our results offer new insights into the fundamental understanding of Atlantic blocking activity. We should consider the remote impacts of the Pacific when evaluating long-term variations and future changes in Atlantic blocking activity under realistic orography.

Table 1. List of semi-idealised atmospheric-only experiments.

Experiment	Tropical SST	Extratropical Atlantic SST	Extratropical Pacific SST
Zonally uniform tropical SST/No front (ZUNF).	Zonally Uniform	No front	No front
Realistic SST forcing in Northern Hemisphere and tropics (FULL)	Realistic	Realistic	Realistic
Realistic extratropical SST forcing (EXT_ALL)	Zonally Uniform	Realistic	Realistic
Realistic tropical SST forcing (TROP_ALL)	Realistic	No front	No front
Realistic extratropical Atlantic SST forcing (EXT_ATL)	Zonally Uniform	Realistic	No front
Realistic extratropical Pacific SST forcing (EXT_PAC)	Zonally Uniform	No front	Realistic

METHODS

Numerical experiments

Semi-idealised experiments with different SST configurations prescribed in the MAECHAM5 (the Middle Atmosphere configuration of the fifth generation of the Hamburg version of the ECMWF model) atmospheric-only general circulation model (AGCM) were performed, in order to investigate the atmospheric responses to tropical SST and mid-latitude oceanic fronts; the experiments are listed in Table 1. The experimental design is briefly described below, and the details of these experiments should be referred to ref. ⁴⁴.

The SST in all experiments was derived from the monthly climatology of HadISST for the period 1960–2009. The zonally uniform tropical SST/no-front (ZUNF) run prescribed the monthly-varying zonally uniform SST in all ocean basins, such that the climatological zonal SST gradient over the tropical ocean was removed and the meridional SST gradient in the mid-latitudes (representing the mid-latitude oceanic fronts) over the Pacific and Atlantic was greatly reduced (Supplementary Fig. 10a; see also SFig. 1 in ref. ⁴⁴). Five sensitivity experiments were performed. The difference between the sensitivity experiments and the ZUNF run represent the atmospheric response to prescribing realistic tropical and/or extratropical SST over different ocean basins.

The EXT_ALL run prescribed realistic mid-latitude oceanic fronts over the Atlantic and Pacific Ocean and zonally uniform SST at each latitude over the entire tropical ocean, whereas the TROP_ALL run prescribed realistic tropical SST and zonally uniform SST over the extratropical North Atlantic and North Pacific (Supplementary Fig. 10b). The EXT_ATL run prescribed a realistic Atlantic mid-latitude oceanic front and zonally uniform SST over the extratropical Pacific and the entire tropical ocean (Supplementary Fig. 10c), whereas the EXT_PAC run prescribed a realistic Pacific mid-latitude oceanic front and zonally uniform SST over the extratropical Atlantic and the entire tropical ocean (Supplementary Fig. 10d). The FULL run prescribed realistic tropical SST and the mid-latitude SST fronts in the North Pacific and the North Atlantic.

Reanalysis datasets

Daily archives of the NCEP/NCAR reanalysis datasets⁴⁸ for the period of 1960 through 2009 were obtained to assess the ability of the FULL run to simulate the large-scale circulation features and the blocking activity.

Blocking index

Blocking was detected by the reversal of the meridional geopotential height gradient¹⁵, where over the extratropical region the geopotential height gradient in the north (GHGN) (Eq. 1) is strongly negative and the geopotential height gradient in

the south (GHGS) (Eq. 2) is positive:

$$\text{GHGN}(\lambda, \varphi_0, t) = \frac{Z_{500}(\lambda, \varphi_N, t) - Z_{500}(\lambda, \varphi_0, t)}{\varphi_N - \varphi_0} \quad (1)$$

$$\text{GHGS}(\lambda, \varphi_0, t) = \frac{Z_{500}(\lambda, \varphi_0, t) - Z_{500}(\lambda, \varphi_S, t)}{\varphi_0 - \varphi_S} \quad (2)$$

where the gradients were computed over 15 degrees of latitude, with $\varphi_N \in [50, 90]^\circ N$, $\varphi_0 \in [35, 75]^\circ N$, $\varphi_S \in [20, 60]^\circ N$. On a calendar date t , a grid is called a blocking grid when $\text{GHGN} < -10$ gpm and $\text{GHGS} > 0$ gpm. In addition to fulfilling the reversal criterion, the blocking high should be large and persistent. For the size criterion, a blocking region (i.e. all grids inside the region are blocking grids) should be larger than 1×10^6 km². When the blocking regions in two consecutive calendar dates overlap, it is considered a blocking event. The first and last dates of a blocking event satisfying the above blocking criteria are called the onset date (day+0) and the lysis date, respectively. We analyse only the blocking events persisting for at least four consecutive days.

Geopotential height tendency equation

The geopotential height tendency equation at 500 hPa^{49,50} is used to diagnose certain physical processes related to the evolution of blocking events; the derivation of the full equation can be seen in ref. ⁶⁹ and is also briefly described here. The full form of the geopotential height tendency is attributed mainly to vorticity flux divergence, which is the sum of horizontal vorticity advection and vorticity divergence.

$$\frac{\partial Z_{500}}{\partial t} \approx -\frac{f}{g} \nabla^{-2} (\nabla_H \cdot (\mathbf{V} \xi_a)) = -\frac{f}{g} \nabla^{-2} (\mathbf{V} \cdot \nabla_H \xi_a - \xi_a \nabla_H \cdot \mathbf{V}) \quad (3)$$

where f denotes the Coriolis parameter, g denotes the acceleration due to gravitation, \mathbf{V} represents the vector wind, and ξ_a represents the absolute vorticity.

Each physical quantity in Eq. (3) is then decomposed into climatological mean, high-frequency transient eddies, and low-frequency transient eddies, where the vorticity flux divergence is expressed as:

$$\begin{aligned} \nabla_H \cdot (\mathbf{V} \xi_a) = & \underbrace{-\nabla_H \cdot (\overline{\mathbf{V} \xi_a})}_{(i)} - \underbrace{\nabla_H \cdot (\mathbf{V}'_{HP} \xi'_{HP})}_{(ii)} - \underbrace{\nabla_H \cdot (\overline{\mathbf{V}'_{HP} \xi_a} + \mathbf{V}'_{HP} \overline{\xi_a})}_{(iii)} \\ & - \underbrace{\nabla_H \cdot (\mathbf{V}'_{LP} \xi'_{LP})}_{(iii)} - \underbrace{\nabla_H \cdot (\overline{\mathbf{V}'_{LP} \xi_a} + \mathbf{V}'_{LP} \overline{\xi_a})}_{(iii)} - \underbrace{\nabla_H \cdot (\mathbf{V}'_{HP} \xi'_{LP} + \mathbf{V}'_{LP} \xi'_{HP})}_{(iv)} \end{aligned} \quad (4)$$

where the overbar represents the daily climatological mean, the prime represents an anomaly (i.e., a local departure from the daily climatological mean); and the subscripts HP and LP denote 8-day high-pass and low-pass filtered anomalies, respectively, based on a 101-point Lanczos filter. Therefore, terms (i)–(iv) in Eq. (4) represent the contributions from the climatological mean, the high-frequency transient eddies, the low-frequency transient

eddies, and the cross-frequency component, respectively. This decomposition is similar to that in ref. ¹⁷.

Derivation of the geopotential height tendency equation

The geopotential height tendency equation at 500 hPa^{49,60,68} is used to diagnose the major physical processes during the evolution of blocking events. The equation is derived from the hydrostatic equation:

$$\partial p / \partial Z = -(p/R_d T)g \quad (5)$$

where g is the acceleration due to gravity ($=9.8 \text{ ms}^{-2}$), T is air temperature, R_d is the gas constant of dry air ($=287 \text{ J K}^{-1} \text{ kg}^{-1}$), and p refers to an arbitrary isobaric level.

Integrating Eq. (5) from the lowest isobaric level (p_l , say 1000 hPa) to p , applying a Laplacian operator [$\nabla^2 = \partial^2 / (\cos \phi \partial \lambda)^2 + \partial^2 / \partial \phi^2$] to Eq. (5), and dividing it by the Coriolis parameter ($f = 2\Omega \sin \phi$; $\Omega = 2\pi/86,400 \text{ s}^{-1}$) gives:

$$\frac{g}{f} \nabla^2 Z = \frac{g}{f} \nabla^2 Z_l + \frac{R_d}{f} \int_{p_l}^p \nabla^2 T \frac{\partial p}{p} \quad (6)$$

Taking a time derivative of Eq. (6) gives:

$$\frac{g}{f} \nabla^2 \frac{\partial Z}{\partial t} = \frac{g}{f} \nabla^2 \frac{\partial Z_l}{\partial t} - \frac{R_d}{f} \int_{p_l}^p \nabla^2 \frac{\partial T}{\partial t} \frac{\partial p}{p} \quad (7)$$

Substituting $\nabla^2 Z$ in Eq. (7) by geostrophic vorticity (ξ_g) obtains:

$$\frac{\partial \xi_g}{\partial t} = \frac{\partial \xi_{gl}}{\partial t} + \frac{R_d}{f} \int_{p_l}^p \nabla^2 \frac{\partial T}{\partial t} \frac{\partial p}{p} \quad (8)$$

At each isobaric level, the tendencies of ξ_g and T in a spherical coordinate system (λ, ϕ, p) can be expressed as:

$$\begin{aligned} \frac{\partial \xi_g}{\partial t} = & \underbrace{-\frac{1}{a} \left(u \frac{\partial \xi_a}{\cos \phi \partial \lambda} + v \frac{\partial \xi_a}{\partial \phi} \right)}_{(i)} - \underbrace{\frac{1}{a} \left(u \frac{\partial \xi_a}{\cos \phi \partial \lambda} + v \frac{\partial \xi_a}{\partial \phi} \right)}_{(i)} \\ & - \underbrace{\frac{1}{a} \left(\frac{\partial w}{\cos \phi \partial \lambda} \frac{\partial v}{\partial p} - \frac{\partial w \partial v}{\partial \phi \partial p} \right)}_{(iv)} + \underbrace{\frac{1}{a} \left(\frac{\partial F}{\cos \phi \partial \lambda} + \frac{\partial F}{\partial \phi} \right)}_{(v)} - \underbrace{\frac{\partial \xi_{ag}}{\partial t}}_{(vi)} \end{aligned} \quad (9)$$

$$\frac{\partial T}{\partial t} = \underbrace{-\frac{1}{a} \left(u \frac{\partial T}{\cos \phi \partial \lambda} + v \frac{\partial T}{\partial \phi} \right)}_{(vii)} - \underbrace{w \frac{T}{\theta} \frac{\partial \theta}{\partial p}}_{(viii)} + \underbrace{\frac{\dot{Q}}{c_p}}_{(ix)} \quad (10)$$

where a denotes the earth's radius ($=6.38 \times 10^6 \text{ km}$), u and v refer to the zonal and meridional components of horizontal wind, respectively, w refers to vertical velocity, θ refers to potential temperature, and λ, ϕ , and p represent the longitude, latitude, and pressure level, respectively; terms (i)–(viii) are: (i) horizontal advection of absolute vorticity, (ii) vertical advection of absolute vorticity, (iii) stretching effect, (iv) tilting, (v) frictional effect, (vi) ageostrophic vorticity tendency, (vii) horizontal advection of air temperature; (viii) adiabatic heating, and (ix) diabatic heating, which is taken as the residual of Eq. (10). Note that the friction effect (term v) was found to be too small and is not considered.

After obtaining each of the terms in Eqs. (9) and (10) and putting them into Eq. (8), their contribution to the height tendency at 500 hPa can be obtained by performing an inverse Laplacian (∇^{-2}) for Eq. (8):

$$\begin{aligned} \frac{\partial Z_{500}}{\partial t} = & \nabla^{-2} \left\{ g \times \frac{1}{p_r - p_l} \int_{p_l}^{p_r} [\text{sum of terms (i) to (v) in Eq. 9}] \partial p \right\} \\ & - \nabla^{-2} \left\{ \frac{R_d}{g} \int_{p_l}^{p_r} \left\{ \int_{p_l}^{500} \nabla^2 [\text{sum of terms (vi) to (viii) in Eq. 10}] \frac{\partial p}{p} \right\} \partial p \right\} \end{aligned} \quad (11)$$

where p_l is set at 1000 hPa and p_r is set at 100 hPa.

The 500-hPa height tendency was found to be primarily due to the vorticity flux divergence (terms (i) and (iii) in Eq. (9)). Then, the dynamics of blocking was analysed based on the decomposition of Eq. (3). Note that in the decomposition we only showed the results based on 500 hPa alone and not showing the results based on the data from 1000 hPa to 100 hPa because the results based on these two methods are quantitatively the same.

Plumb flux

The propagation of stationary planetary-wave activity is depicted by the horizontal component of Plumb flux⁷⁰, which in a spherical coordinate system (λ, ϕ, p) can be expressed as:

$$F_S = p \cos \phi \left(\frac{1}{2a^2 \cos^2 \phi} \left[\left(\frac{\partial \psi'}{\partial \lambda} \right)^2 - \psi' \frac{\partial^2 \psi'}{\partial \lambda^2} \right] - \frac{1}{2a^2 \cos^2 \phi} \left[\frac{\partial \psi'}{\partial \lambda} \frac{\partial \psi'}{\partial \phi} - \psi' \frac{\partial^2 \psi'}{\partial \lambda \partial \phi} \right] \right) \quad (12)$$

where the streamfunction $\psi = Z/2\Omega \sin \phi$, where Ω is the Earth's rotation rate. Note that the prime in Eq. (12) indicates the zonally asymmetric component.

DATA AVAILABILITY

All data sources are mentioned in the Methods section. The datasets analysed in this study are available from the corresponding authors upon reasonable request.

CODE AVAILABILITY

The codes used to generate the results in the manuscript are available from the corresponding authors upon reasonable request.

Received: 19 December 2021; Accepted: 15 May 2023;

Published online: 06 June 2023

REFERENCES

- Dole, R. M. & Gordon, N. D. Persistent anomalies of the extratropical Northern Hemisphere wintertime circulation: Geographical distribution and regional persistence characteristics. *Mon. Wea. Rev.* **111**, 1567–1586 (1983).
- Tibaldi, S. & Molteni, F. On the operational predictability of blocking. *Tellus* **42A**, 343–365 (1990).
- Pelly, J. L. & Hoskins, B. J. A new perspective on blocking. *J. Atmos. Sci.* **60**, 743–755 (2003).
- Takaya, K. & Nakamura, H. Mechanisms of intraseasonal amplification of the cold Siberian High. *J. Atmos. Sci.* **62**, 4423–4440 (2005).
- Zhou, W. et al. Synoptic-scale controls of persistent low temperature and icy weather over southern China in January 2008. *Mon. Wea. Rev.* **137**, 3978–3991 (2009).
- Buehler, T., Raible, C. C. & Stocker, T. F. The relationship of winter season North Atlantic blocking frequencies to extreme cold or dry spells in the ERA-40. *Tellus* **63A**, 212–222 (2011).
- Sillmann, J., Croci-Maspoli, M., Kallache, M. & Katz, R. W. Extreme cold winter temperatures in Europe under the influence of North Atlantic atmospheric blocking. *J. Clim.* **24**, 5899–5913 (2011).
- Pfahl, S. & Wernli, H. Quantifying the relevance of atmospheric blocking for co-located temperature extremes in the Northern Hemisphere on (sub-) daily time scales. *Geophys. Res. Lett.* **39**, L12807 (2012).
- Scaife, A., Woollings, T., Knight, J., Martin, G. & Hinton, T. Atmospheric blocking and mean biases in climate models. *J. Clim.* **23**, 6143–6152 (2010).
- Dunn-Sigouin, E. & Son, S.-W. Northern Hemisphere blocking frequency and duration in the CMIP5 models. *J. Geophys. Res.* **118**, 1179–1188 (2013).
- Cheung, H. H. N. & Zhou, W. Implications of Ural blocking for East Asian winter climate in CMIP5 GCMs. Part I: Biases in the historical scenario. *J. Clim.* **28**, 2203–2216 (2015).
- Davini, P. & D'Andrea, F. From CMIP3 to CMIP6: Northern hemisphere atmospheric blocking. *J. Clim.* **33**, 10021–10038 (2020).
- Schiemann, R. et al. Northern Hemisphere blocking simulation in current climate models: evaluating progress from the Climate Model Intercomparison Project Phase 5 to 6 and sensitivity to resolution. *Weather Clim. Dynam.* **1**, 277–292 (2020).

14. Woollings, T. et al. Blocking and its response to climate change. *Curr. Clim. Change Rep.* **4**, 287–300 (2018).
15. Scherrer, S. C., Croci-Maspoli, M., Schwierz, C. & Appenzeller, C. Two-dimensional indices of atmospheric blocking and their statistical relationship with winter climate patterns in the Euro-Atlantic region. *Int. J. Climatol.* **26**, 233–249 (2006).
16. Nakamura, H. & Wallace, J. M. Synoptic behavior of baroclinic eddies during the blocking onset. *Mon. Wea. Rev.* **127**, 1892–1903 (1993).
17. Hwang, J., Martineau, P., Son, S.-W., Miyasaka, T. & Nakamura, H. The role of transient eddies in North Pacific blocking formation and its seasonality. *J. Atmos. Sci.* **77**, 2453–2470 (2020).
18. Nakamura, H., Sampe, T., Tanimoto, Y. & Shimpo, A. Observed associations among storm tracks, jet streams and midlatitude oceanic fronts. *Geophys. Monogr. Ser.* **147**, 329–345 (2004).
19. Scaife, A. A. et al. Improved Atlantic winter blocking in a climate model. *Geophys. Res. Lett.* **38**, L23703 (2011).
20. Athanasiadis, P. J. et al. Mitigating climate biases in the mid-latitude North Atlantic by increasing model resolution: SST gradients and their relation to blocking and the jet. *J. Clim.* **35**, 3385–3406 (2022).
21. Bjerknes, J. Atlantic air-sea interaction. *Adv. Geophys.* **10**, 1–82 (1964).
22. Frankignoul, C. Sea surface temperature anomalies, planetary waves and air-sea feedback in the middle latitudes. *Rev. Geophys.* **23**, 357–390 (1985).
23. Rodwell, M. J. & Folland, C. K. Atlantic air-sea interaction and seasonal predictability. *Q. J. R. Meteorol. Soc.* **128**, 1413–1443 (2002).
24. Esbensen, S. K. & Reynolds, R. W. Estimating monthly averaged air-sea transfers of heat and momentum using the bulk aerodynamic method. *J. Phys. Oceanology* **11**, 457–465 (1981).
25. Hasselmann, K. Stochastic Climate Models.1. Theory. *Tellus* **28**, 473–485 (1976).
26. Eden, C. & Jung, T. North Atlantic interdecadal variability: oceanic response to the North Atlantic Oscillation (1865–1997). *J. Clim.* **14**, 676–691 (2001).
27. Eden, C. & Willebrand, J. Mechanism of interannual to decadal variability of the North Atlantic circulation. *J. Clim.* **14**, 2266–2280 (2001).
28. Visbeck, M. et al. The ocean's response to North Atlantic Oscillation variability in "The North Atlantic Oscillation". In (eds Hurrell J. W. et al.) *The North Atlantic Oscillation: Climate significance and environmental impact*. American Geophysical Union, pp 113–146 (Washington, DC, 2003).
29. Li, J., Sun, C. & Jin, F.-F. NAO implicated as a predictor of Northern Hemisphere mean temperature multidecadal variability. *Geophys. Res. Lett.* **40**, 5497–5502 (2013).
30. Omrani, N.-E. et al. Coupled stratosphere-troposphere-Atlantic multidecadal oscillation and its importance for near-future climate projection. *npj Clim. Atmos. Sci.* **5**, 59 (2022).
31. Minobe, S., Kuwano-Yoshida, A., Komori, N., Xie, S.-P. & Small, R. J. Influence of the Gulf Stream on the troposphere. *Nature* **452**, 206–210 (2008).
32. Kwon, Y.-O. et al. Role of the Gulf Stream and Kuroshio-Oyashio systems in large-scale atmosphere-ocean interaction: a review. *J. Clim.* **23**, 3249–3281 (2010).
33. Small, R. J., Tomas, R. A. & Bryan, F. O. Storm track response to ocean fronts in a global high-resolution climate model. *Clim. Dyn.* **43**, 805–828 (2014).
34. Lee, R. W. et al. Impact of Gulf Stream SST biases on the global atmospheric circulation. *Clim. Dyn.* **51**, 3369–3387 (2018).
35. O'Reilly, C. H., Minobe, S. & Kuwano-Yoshida, A. The influence of the Gulf Stream on wintertime European blocking. *Clim. Dyn.* **47**, 1545–1567 (2016).
36. Woollings, T., Hoskins, B., Blackburn, M. & Berrisford, P. A new Rossby wave-breaking interpretation of the North Atlantic Oscillation. *J. Atmos. Sci.* **65**, 609–626 (2008).
37. Wilson, C., Sinha, B. & Williams, R. G. The effect of ocean dynamics and orography on atmospheric storm tracks. *J. Clim.* **22**, 3689–3702 (2009).
38. Joyce, T. M., Kwon, Y.-O., Seo, H. & Ummerhofer, C. C. Meridional Gulf Stream shifts can influence wintertime variability in the North Atlantic storm track and Greenland blocking. *Geophys. Res. Lett.* **46**, 1702–1708 (2019).
39. Honda, M., Nakamura, H., Ukita, J., Kousaka, I. & Takeuchi, K. Interannual seesaw between the Aleutian and Icelandic Lows. Part I: Seasonal dependence and life cycle. *J. Clim.* **14**, 1029–1042 (2001).
40. Merkel, U. & Latif, M. A high resolution AGCM study of the El Niño impact on the North Atlantic/European sector. *Geophys. Res. Lett.* **29**, 1291 (2002).
41. Graf, H.-F. & Zanchettin, D. Central Pacific El Niño, the "subtropical bridge" and Eurasian climate. *J. Geophys. Res.* **117**, D01102 (2012).
42. Ding, Q. et al. Tropical forcing of the recent rapid Arctic warming in northeastern Canada and Greenland. *Nature* **509**, 209–212 (2014).
43. Hardiman, S. C. et al. The impact of strong El Niño and La Niña events on the North Atlantic. *Geophys. Res. Lett.* **46**, 2874–2883 (2019).
44. Omrani, N.-E. et al. Key role of the ocean western boundary currents in shaping the Northern Hemisphere climate. *Sci. Rep.* **9**, 3014 (2019).
45. Horel, J. D. & Wallace, J. M. Planetary-scale atmospheric phenomena associated with the southern oscillation. *Mon. Wea. Rev.* **109**, 813–829 (1981).
46. Li, Y. & Lau, N.-C. Impact of ENSO on the atmospheric variability over the North Atlantic in late winter—Role of transient eddies. *J. Clim.* **25**, 320–342 (2012).
47. Yamamoto, A. et al. Oceanic moisture sources contributing to wintertime Euro-Atlantic blocking. *Wea. Clim. Dyn.* **2**, 819–840 (2021).
48. Kalnay, E. et al. The NCEP/NCAR 40-year reanalysis project. *Bull. Am. Met. Soc.* **77**, 437–471 (1996).
49. Tsou, C.-H. & Smith, P. J. The role of synoptic/planetary-scale interaction during the development of a blocking anticyclone. *Tellus* **42A**, 174–193 (1990).
50. Lupo, A. R. & Smith, P. J. Planetary and synoptic-scale interactions during the life cycle of a mid-latitude blocking anticyclone over the North Atlantic. *Tellus* **47A**, 575–596 (2001).
51. Illari, L. & Marshall, J. C. On the interpretation of eddy fluxes during a blocking episode. *J. Atmos. Sci.* **40**, 2232–2242 (1983).
52. Shutts, G. J. A case study of eddy forcing during an Atlantic blocking episode. *Adv. Geophys.* **29**, 135–162 (1986).
53. Nakamura, H., Nakamura, M. & Anderson, J. L. The role of high- and low-frequency dynamics in blocking formation. *Mon. Wea. Rev.* **125**, 2074–2093 (1997).
54. Colucci, S. J. Planetary-scale preconditioning for the onset of blocking. *J. Atmos. Sci.* **58**, 933–942 (2001).
55. Tyrllis, E. & Hoskins, B. J. The morphology of Northern Hemisphere blocking. *J. Atmos. Sci.* **65**, 1653–1665 (2008).
56. Hotta, D. & Nakamura, H. On the significance of sensible heat supply from the ocean in the maintenance of the mean baroclinicity along storm tracks. *J. Clim.* **24**, 3377–3401 (2011).
57. Lindzen, R. S. & Farrell, B. A simple approximate result for the maximum growth rate of baroclinic instabilities. *J. Atmos. Sci.* **37**, 1648–1654 (1980).
58. Nakamura, H., Sampe, T., Goto, A., Ohfuchi, W. & Xie, S.-P. On the importance of midlatitude oceanic frontal zones for the mean state and dominant variability in the tropospheric circulation. *Geophys. Res. Lett.* **35**, L15709 (2008).
59. Hoskins, B. J. & Hodges, K. I. New perspectives on the Northern Hemisphere winter storm tracks. *J. Atmos. Sci.* **59**, 1041–1061 (2002).
60. Chang, E. K. M. Are band-pass variance statistics useful measures of storm track activity? Re-examining storm track variability associated with the NAO using multiple storm track measures. *Clim. Dyn.* **33**, 277–296 (2009).
61. Brayshaw, D. J., Hoskins, B. & Blackburn, M. The basic ingredients of the North Atlantic storm track. Part II: Sea surface temperature. *J. Atmos. Sci.* **68**, 1784–1805 (2011).
62. Hoskins, B. J., James, I. N. & White, G. H. The shape, propagation and mean-flow interaction of large-scale weather systems. *J. Atmos. Sci.* **40**, 1595–1612 (1983).
63. Valdes, P. J. & Hoskins, B. J. Nonlinear orographically forced planetary waves. *J. Atmos. Sci.* **48**, 2089–2106 (1991).
64. Lee, S. & Kim, H.-Y. The dynamical relationship between subtropical and eddy-driven jets. *J. Atmos. Sci.* **60**, 1490–1503 (2003).
65. Wallace, J. M. & Gutzler, D. S. Teleconnections in the geopotential height field during the Northern Hemisphere winter. *Mon. Wea. Rev.* **109**, 784–812 (1981).
66. Berckmans, J., Woollings, T., Demory, M.-E., Vidale, P.-L. & Roberts, M. Atmospheric blocking in a high resolution climate model: influences of mean state, orography and eddy forcing. *Atmos. Sci. Lett.* **14**, 34–40 (2013).
67. Held, I. M., Ting, M. & Wang, H. Northern winter stationary waves: theory and modeling. *J. Clim.* **15**, 2125–2144 (2002).
68. Ren, R., Xia, X. & Rao, J. Topographic forcing from East Asia and North America in the northern winter stratosphere and their mutual interference. *J. Clim.* **32**, 8639–8658 (2019).
69. Lupo, A. R., Smith, P. J. & Zwack, P. A diagnosis of the explosive development of two extratropical cyclones. *Mon. Wea. Rev.* **120**, 1490–1523 (1992).
70. Plumb, R. A. On the three-dimensional propagation of stationary waves. *J. Atmos. Sci.* **42**, 217–229 (1985).

ACKNOWLEDGEMENTS

The authors greatly appreciate the constructive comments provided by the three anonymous reviewers. HNC acknowledges support from the National Natural Science Foundation of China (Grant No. 41905050), the Innovation Group Project of the Southern Marine Science and Engineering Guangdong Laboratory (Zhuhai) (#311021001), and the Guangdong Province Key Laboratory for Climate Change and Natural Disaster Studies (Grant No. 2020B1212060025). The Bjerknes Climate Prediction Unit with funding from the Trond Mohn Foundation (grant BFS2018TMT01) supported NOE and NK. NOE acknowledges support from the Research Council of Norway (Grant No. 312017, RACE; Grant No. 316618, ROADMAP) through JPI Climate & JPI Oceans Joint Transnational Call on Next Generation Climate Sciences in Europe for Oceans and Belmont Forum. NK acknowledges support from the Research Council of Norway (Grant No. 328935, COMBINED) and the Ministry of Science and Higher Education of the Russian Federation (Agreement No. 075–15–2021–577). HN is supported in part by the Japanese Ministry of Education, Culture, Sports, Science and Technology through the Arctic Challenge for

Sustainability (ArCS-II), by the Japan Science and Technology Agency through COI-NEXT JPMJPF2013, by the Environmental Restoration and Conservation Agency of Japan through the Environment Research and Technology Development Fund JPMEERF20222002, and by the Japan Society for the Promotion of Science through Grants-in-Aid for Scientific Research 19H05702 (on Innovative Areas 6102), 20H01970 and 22H01292. WZ acknowledges support from the Research Grants Council of the Hong Kong Special Administrative Region, China (Grant No. 11300920).

AUTHOR CONTRIBUTIONS

H.-N.C. and N.-E.O. initiated this research. H.-N.C. performed the data analysis and drafted the manuscript. N.-E.O. and F.O. designed and N.-E.O. performed the numerical experiments. All authors contributed to writing and revising the manuscript.

FUNDING

Open access funding provided by University of Bergen.

COMPETING INTERESTS

The authors declare no competing interests.

ADDITIONAL INFORMATION

Supplementary information The online version contains supplementary material available at <https://doi.org/10.1038/s41612-023-00370-x>.

Correspondence and requests for materials should be addressed to Ho-Nam Cheung or Nour-Eddine Omrani.

Reprints and permission information is available at <http://www.nature.com/reprints>

Publisher's note Springer Nature remains neutral with regard to jurisdictional claims in published maps and institutional affiliations.



Open Access This article is licensed under a Creative Commons Attribution 4.0 International License, which permits use, sharing, adaptation, distribution and reproduction in any medium or format, as long as you give appropriate credit to the original author(s) and the source, provide a link to the Creative Commons license, and indicate if changes were made. The images or other third party material in this article are included in the article's Creative Commons license, unless indicated otherwise in a credit line to the material. If material is not included in the article's Creative Commons license and your intended use is not permitted by statutory regulation or exceeds the permitted use, you will need to obtain permission directly from the copyright holder. To view a copy of this license, visit <http://creativecommons.org/licenses/by/4.0/>.

© The Author(s) 2023